A Point-of-Care Sensing Platform for Multiplexed Detection of Chronic Kidney Disease Biomarkers Using Molecularly Imprinted Polymers

Yixuan Li, Liuxiong Luo, Yingqi Kong, Sophiamma George, Yujia Li, Xiaotong Guo, Xin Li, Eric Yeatman, Andrew Davenport, Ying Li, and Bing Li*

Chronic kidney disease (CKD) is one of the most serious non-communicable diseases affecting the population. In the early-stages patients have no obvious symptoms, until it becomes life-threatening leading end-stage kidney failure. Therefore, it is important to early diagnose CKD to allow therapeutic interventions and progression monitoring. Here, a point-of-care (POC) sensing platform is reported for the simultaneous detection of three CKD biomarkers, namely creatinine, urea, and human serum albumin (HSA), using reduced graphene oxide/polydopamine-molecularly imprinted polymer (rGO/PDA-MIP) fabricated with novel surface-molecularly imprinting technology. A multi-channel electrochemical POC readout system with differential pulse voltammetry (DPV) function is developed, allowing the simultaneous detection of the three biomarkers, in combination with the surface-MIP electrodes. This sensing platform achieves the record low limit-of-detection (LoD) at a femtomolar level for all three analytes, with wide detection ranges covering their physiological concentrations. Clinical validation is performed by measuring these analytes in serum and urine from healthy controls and patients with CKD. The average recovery rate is 81.8–119.1% compared to the results obtained from the hospital, while this platform is more cost-effective, user-friendly, and requires less sample-to-result time, showing the potential to be deployed in resource-limited settings for the early diagnosis and tracking progression of CKD.

1. Introduction

Chronic kidney disease (CKD), which is defined as structural abnormalities, persistent urinary abnormalities, or impaired excretory kidney function, has become one of the most serious non-communicable diseases affecting the adult population worldwide.[1] Patients with early stages of CKD typically report no, or mild non-specific symptoms, whilst those patients with symptoms are most likely to be at advanced stages, when dialysis becomes necessary. Early diagnosis of CKD would allow the implementation of interventions to timely prevent or slow disease progression and so significantly benefit patients' health-related quality of life. Therefore, the development of tools to detect early stages of CKD, and track kidney function by measuring biomarkers in body fluids is of potentially great significance.[2] In clinical practice, some serum and urinary biomarkers have been proven to be discriminative indicators for both diagnosing CKD and monitoring progress. For example, increased concentrations of both creatinine and urea

Y. Li, Y. Kong, Y. Li, B. Li
Institute for Materials Discovery
Department of Chemistry
University College London
London WC1E 7JE, UK
E-mail: bing.li@ucl.ac.uk
L. Luo
School of Materials Science and Engineering
Central South University
Changsha 410083, P. R. China

The ORCID identification number(s) for the author(s) of this article can be found under https://doi.org/10.1002/adfm.202316865

S. George, A. Davenport
Department of Nephrology
Royal Free Hospital
London NW3 2QG, UK
X. Guo, E. Yeatman
Department of Electrical and Electronic Engineering
Imperial College London
London SW7 2AZ, UK
X. Li
School of Finance & Accounting
University of Westminster
London NW1 5LS, UK
A. Davenport
Department of Renal Medicine
University College London
London NW3 2PF, UK

2316865 (1 of 13)

in serum or decreased concentrations in urine;[3] or urinary albumin greater than 30 mg L^{-1}[4] is indicative of underlying kidney disease.[5] The common methods for the measurement of these biomarkers in hospital mainly include the enzymatic method for creatinine analysis,[6] glutamate dehydrogenase for urea detection,[7] and bromocresol green reaction for human serum albumin (HSA) quantification.[8] However, although these analysis strategies can be readily used in hospitals by trained technicians with laboratory equipment designed to measure multiple samples, they lack accuracy due to reactions between reagents and interferents from body fluids. Some other gold standard methods, such as chromatography,[9] are often chosen for the highly precise detection of various biomarkers in the lab. Nonetheless, the expensive equipment and demanding operations make it difficult to implement as point-of-care (POC) detection in primary healthcare and screening settings.[1]

Emerging biosensing technologies have been reported to address this urgent need to create POC diagnostics. There have been picric acid methods for the detection of creatinine,[10,11] Ni-based biosensors for the electrocatalytic detection of urea,[12,13] and immunoturbidimetry assays for the estimation of HSA.[8,14] However, these novel technologies come with a number of limitations, and some of their sensing characteristics limit any potential practical application. For example, the inadequate limit-of-detection (LoD) of colorimetric methods fails to detect the biomarkers with ultra-low concentration in body fluids;[15] the poor selectivity of metal particle recognition strategy might lead to insufficient accuracy for analyte detection;[16] or the prolonged detection durations and delicate operational requirements of immunoturbidimetry method make it challenging for POC detection in resource-limited region.[17] In addition, these methods all focus on the detection of single biomarkers, which reduces the accuracy for ensuring reliable diagnosis, as the individual biomarker profile can be affected by other underlying diseases and conditions.[18] Therefore, it is essential to develop a POC biosensing platform with high sensitivity, selectivity, and low LoD, which more importantly, has the capability for the simultaneous analysis of multiple biomarkers in clinical samples.

Molecularly imprinted polymer (MIP) is a polymeric matrix with cavities, which simulates the interaction between antibody-antigen to bind with the specific biomarkers.[19,20] MIP-based biosensors have been developed over recent years for the ultra-sensitive detection of various biomarkers,[21,22] including creatinine, urea, and HSA,[23–25] with excellent sensitivity and selectivity for direct measurements in clinical samples. However, the intrinsic disadvantages of the traditional MIP biosensors still re-main, mainly with binding sites heterogeneity and slow diffusion mass transfer of analytes to the imprinted sites affecting their overall performance. This results in reduced binding affinity, detection range, and even selectivity, especially for macromolecules, such as protein biomarkers.[26]

In this work, we report on a cost-effective reduced graphene oxide/polydopamine (rGO/PDA)-MIP sensing platform for the simultaneous detection of creatinine, urea, and HSA in both serum and urine, with a huge potential to be deployed into front-line clinical settings. The PDA-MIP layer was synthesized onto the graphene oxide (GO) via surface molecularly imprinting technology. This innovative surface-MIP avoids the deep embedding of template molecules during polymerization by resolving the issue of the excessively thick traditional MIP layers, in turn leading to a wider dynamic detection range. In addition, during the polymerization process, monomer-template complexes react with the GO surface, leading to a partial transition of GO into rGO. The enhanced conductivity of this economical nano-carbon matrix with enhanced surface area further facilitates the rapid electron transfer,[27] and makes this composite exceptionally sensitive for the quantification of target biomarkers. We then integrated the composites with a self-designed miniaturized multi-channel integrated circuit readout system with the function of differential pulse voltammetry (DPV) for detection, empowering it to have the capability to be used by primary healthcare workers as a POC platform.[28] The performance of this POC sensing system has been validated in clinical urine and serum samples against the gold standards in hospital laboratories. The platform shows remarkably high sensitivity, selectivity, robustness, and record LoD at the femtomolar level with an expansive detection range, which makes it a promising approach for screening for CKD and monitoring progression.

2. Results and Discussion

2.1. Overview of Sensing Platform and Fabrication of rGO/PDA-MIP Composites

The rGO/PDA-MIP composites for the detection of the three biomarkers were fabricated using the surface imprinting strategy as shown in **Figure 1A**. Dopamine hydrochloride (DA) has been used as the functional monomer to form hydrogen bonds with the template molecules, namely creatinine, urea, and HSA, to produce respective monomer-template complexes.[29] When the GO dispersion and oxidant ammonium persulfate (AP) were added, relying on the adhesion property of catechol and amine groups which are contained in DA, the complex physically adheres onto the surface of GO and polymerizes, forming a surface-PDA-MIP layer on the GO, with the template frozen in the polymer matrix. During this process, GO is partially reduced to rGO, while DA undergoes oxidation to quinone, which can then be converted to the more readily oxidizable leucodopamine-chrome by intramolecular cyclization via 1,4-Michael addition. The oxidation and intramolecular rearrangement of leucodopamine-chrome forms 5,6-dihydroxyindole and its isomer, which undergoes further polymerization reactions to produce PDA-MIP, a melanin-like polymer with templates embedded.[30] The embedded template molecules are then subsequently removed during the elution process, with the binding cavities retaining their size,

Y. Li
Department of Brain Repair and Rehabilitation
UCL Institute of Neurology
London WC1N 3BG, UK

B. Li
Care Research & Technology Centre
UK Dementia Research Institute
London W12 0BZ, UK

B. Li
Department of Brain Science
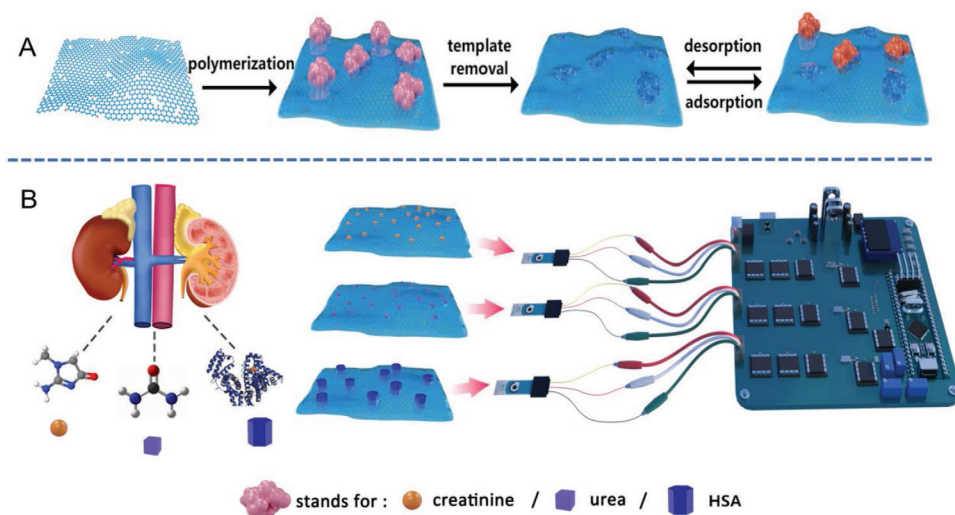Imperial College London
London W12 0BZ, UK

Figure 1. Overview of the surface-MIP synthesis and its detection process based on the designed multiplexed POC sensing platform. A) The preparation and recognition process of surface-MIP (rGO/PDA-MIP) composites. B) Workflow of the simultaneous detection of creatinine, urea, and HSA using MIP-based electrochemical sensor with self-designed POC readout.

shape, and function complementary to the targets, thus obtaining rGO/PDA-MIP composites with specific recognition capabilities to their target molecules. Creatinine, urea, and HSA have been selected as a specific combination for the diagnosis of CKD. In this project, these three biomarkers were simultaneously analyzed through the rGO/PDA-MIP modified screen-printed electrochemical sensors, which are interfaced with a miniaturized multi-channel integrated circuit readout system, as shown in Figure 1B.

A systematic optimization was conducted to elucidate factors influencing the performance of rGO/PDA-MIP modified electrodes, with a particular focus on the mass ratio of templates to monomers and the incubation duration of modified electrodes in analyte solution. The mass ratio of templates to monomers will affect the MIP thickness, as well as the number of imprinted cavities within the polymer matrix. The increased polymer thickness and the reduced number of imprinted cavities can result in a diminished current change (ΔI) (difference between the DPV peak current value detected with the presence of the target in corresponding concentration and in the absence) during evaluations, which results in insufficient sensitivity and a smaller detection range.[31] As depicted in Figure S1A (Supporting Information), variations in the mass ratio of templates to monomers lead to conspicuous alterations in ΔI, where the ΔIs peak at the ratio of 7:8, 3:4, 3:8 for rGO/PDA-MIP (creatinine), (urea), and (HSA) respectively. This means that the recognition ability of fabricated composites to corresponding targets was maximum when the amounts of templates were 35, 30, and 22.5 mg, respectively. This is because an insufficient number of templates will result in fewer imprinting cavities, while excessive templates could hinder the monomer polymerization, resulting in a lower amount of binding cavities, which in turn reduces the detection effectiveness of the MIP to capturing templates.[32]

Figure S1B (Supporting Information) explores the influence of varying incubation time on DPV response for the detection of the three target molecules at the concentration of 1 ng mL^{-1} respectively. The ΔI associated with rGO/PDA-MIP modified electrodes

for the detection of creatinine, urea, and HSA progressively augmented with the incubation time and saturated approximately at 10 min mark. This suggests that the targets combine with the imprinting cavities within the initial minutes, eventually achieving a dynamic equilibrium between the adsorption and desorption processes.[33] The optimum parameters for the fabrication and utilization of rGO/PDA-MIP composites are summarized in **Table 1**.

Based on the optimized recipe, the adsorption capacities of fabricated MIPs were evaluated, with imprinting factors calculated with Equations (1) and (2):

$$Q = \frac{(C_i - C_f)}{m} V \tag{1}$$

$$IF = \frac{Q_{MIP}}{Q_{NIP}} \tag{2}$$

C_i is the initial concentration of the analyte, C_f is the equilibrium concentration of the analyte in solution, m is the mass of the composite, and V is the volume of the solution.

As shown in Figure S2 (Supporting Information), the concentrations of target analytes detected with Ultraviolet–visible spectroscopy (UV–Vis) between the solution after MIPs and non-MIPs (NIPs) adsorption show significant differences. Based on the ratio of MIPs and NIPs adsorption capacity, the imprinting

Table 1. Optimum parameters for fabrication and utilization of rGO/PDA-MIP composites.

	rGO/PDA-MIP (creatinine)	rGO/PDA-MIP (urea)	rGO/PDA-MIP (HSA)
Amount of monomers	40 mg	40 mg	60 mg
Amount of templates	35 mg	30 mg	22.5 mg
Mass ratio of templates/monomers	7:8	3:4	3:8
Incubation time	10 min	10 min	10 min

**ADVANCED
SCIENCE NEWS**

www.advancedsciencenews.com

**ADVANCED
FUNCTIONAL
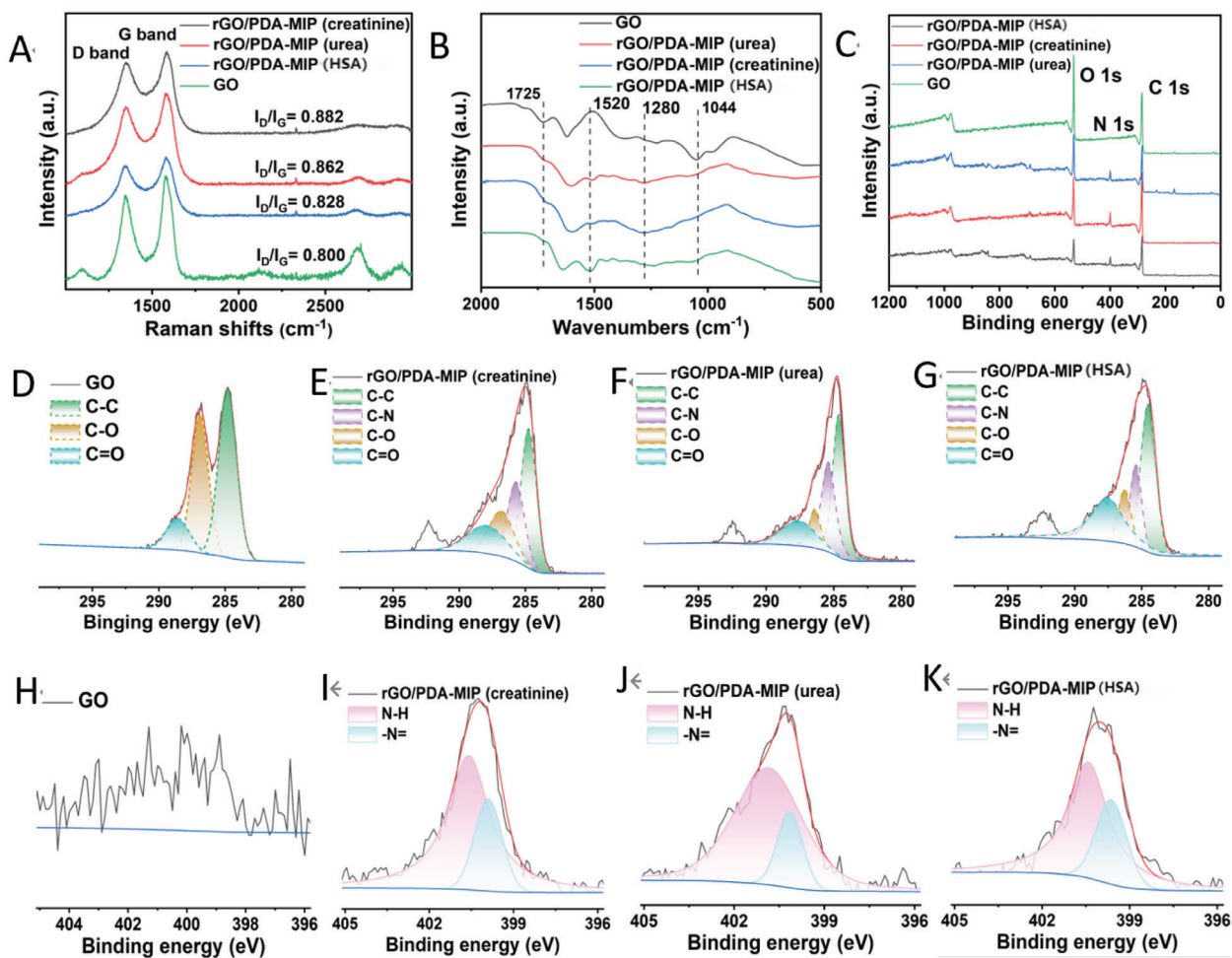MATERIALS**

www.afm-journal.de

Figure 2. Characterization of GO and rGO/PDA-MIP composites using Raman, FTIR, and XPS. A) Raman spectra of GO and rGO/PDA-MIP composites; B) FTIR spectrum of GO and rGO/PDA-MIP composites; C) Full range XPS spectra of GO and rGO/PDA-MIP composites; with XPS C1s spectra of D) GO, E) rGO/PDA-MIP (creatinine), F) rGO/PDA-MIP (urea), G) rGO/PDA-MIP (HSA); XPS N1s spectra of H) GO, I) rGO/PDA-MIP (creatinine), J) rGO/PDA-MIP (urea), K) rGO/PDA-MIP (HSA).

factors of rGO/PDA-MIP (creatinine/urea/HSA) were calculated as 4.9, 3.9, and 7.3, respectively, indicating excellent affinity of fabricated MIPs to target molecules. (NIPs were synthesized under similar conditions with MIPs in the absence of the corresponding template molecules).

2.2. Characterization of rGO/PDA-MIP Composites

To ascertain the successful encapsulation of PDA on the GO, several characterizations including Raman spectroscopy, Fourier transform infrared spectroscopy (FTIR), and X-ray photoelectron spectroscopy (XPS) have been performed on the complex. The Raman spectral analysis, as depicted in **Figure** 2A, reveals two prominent bands for GO, namely the D band (corresponding to defective $sp3$-hybridized carbon atoms) and the G band (indicative of the E_{2g} vibration of $sp2$-hybridized graphitized carbon atoms) at 1344 and 1570 cm^{-1} respectively, with the intensity ratio of D peak to G peak (I_D/I_G) of 0.80.[34,35] Subsequent to the PDA encapsulation, there are observable increases in the I_D/I_G

ratios of rGO/PDA-MIP composites (creatinine/urea/HSA), exhibiting values of 0.882, 0.862, and 0.828, respectively. This alteration is attributed to the cleavage of the oxygen-containing groups on GO during the polymerization process,[36] which contributes to deprotonating the hydroxyl functional group in DA catechol.[37] Moreover, as presented in Figure 2B, a comparative analysis between the FTIR spectra of GO and rGO/PDA-MIP composites underscores a discernible attenuation or disappearance of oxygenated peaks after PDA-coating, including the C—O peak at 1044 cm^{-1} and the C = O peak at 1725 cm^{-1}. Furthermore, the distinctive peaks observed at 1280 and 1520 cm^{-1} are ascribed to the C—N and N—H bonds respectively, which are characteristic of the amide group of PDA.[38]

XPS has been employed to further confirm the above deduction. As illustrated in Figure 2C, the C1s, N1s, and O1s spectrums were compared between GO and fabricated rGO/PDA-MIP composites. Notably, GO is devoid of the N element, which is further corroborated by the XPS N1s spectrum of GO shown in Figure 2H. Figure 2D presents the XPS C1s spectrum of GO, which reveals three peaks located at 284.5, 286.4, and 287.7 eV,
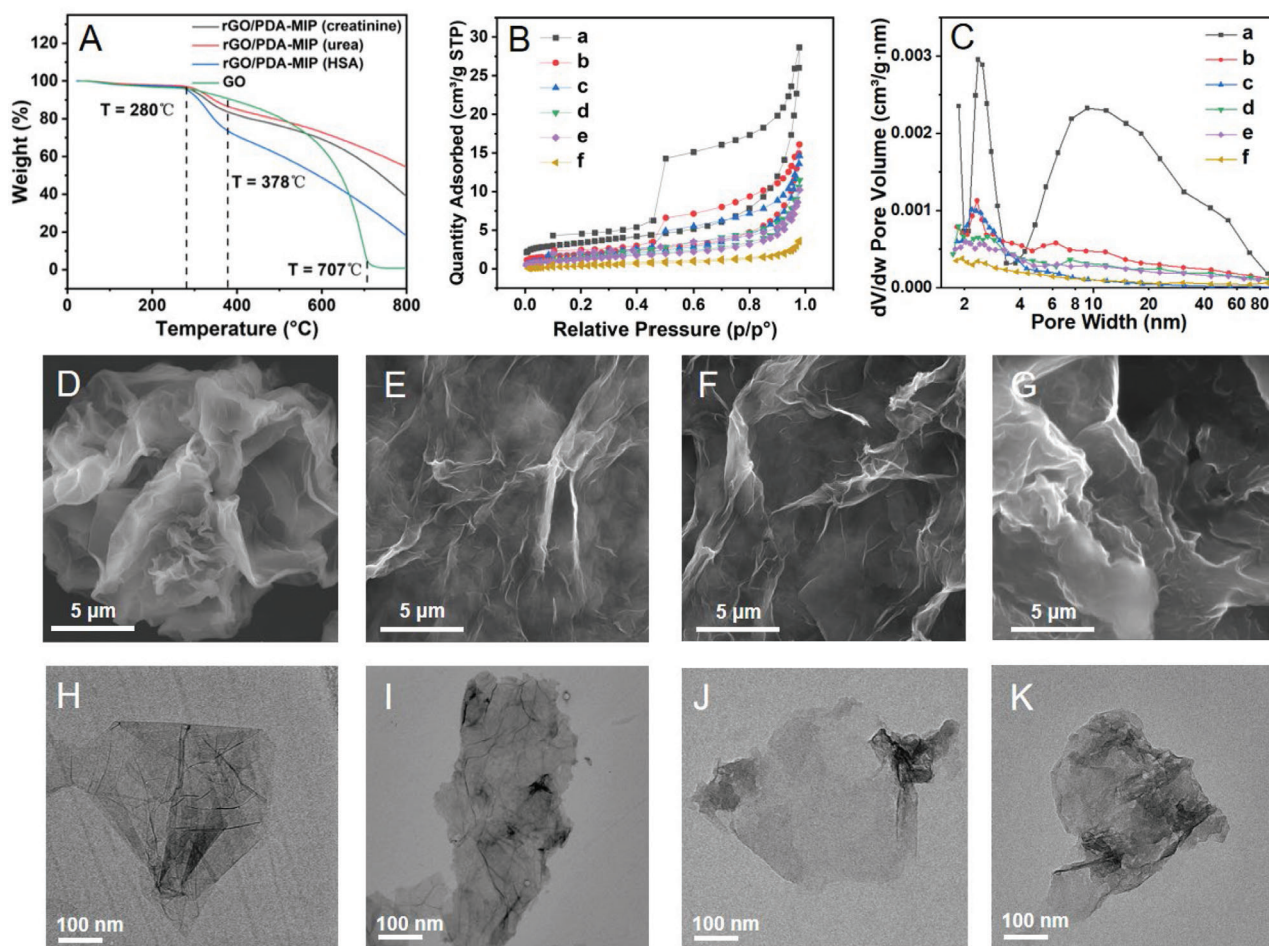
Figure 3. Characterization of GO and rGO/PDA-MIP composites using TGA, BET, SEM, and TEM. A) TGA plot of GO and rGO/PDA-MIP composites; B) Nitrogen adsorption–desorption isotherm of rGO/PDA-MIP and rGO/PDA-NIP composites, where a: rGO/PDA-MIP (HSA), b: rGO/PDA-MIP (creatinine), c: rGO/PDA-MIP (urea), d: rGO/PDA-NIP (HSA), e: rGO/PDA-NIP (creatinine), f: rGO/PDA-NIP (urea); C) Pore size distribution of rGO/PDA-MIP and rGO/PDA-NIP composites, where a: rGO/PDA-MIP (HSA), b: rGO/PDA-MIP (creatinine), c: rGO/PDA-MIP (urea), d: rGO/PDA-NIP (HSA), e: rGO/PDA-NIP (creatinine), f: rGO/PDA-NIP (urea); SEM images of D) GO, E) rGO/PDA-MIP (creatinine), F) rGO/PDA-MIP (urea), G) rGO/PDA-MIP (HSA); TEM images of H) GO, I) rGO/PDA-MIP (creatinine), J) rGO/PDA-MIP (urea), K) rGO/PDA-MIP (HSA).

ascribed to the C—C, C—O, and C=O bonds, respectively.[3,39] The XPS C1s spectra of rGO/PDA-MIP composites in Figure 2E,G show declined intensities of C—O peaks at 286.4 eV and the emergence of C—N peaks at 285.3 eV. This is attributed to the reduction of GO during the PDA polymerization and the appearance of the polymer layer on it. Additionally, a discernible peak at 292.1 eV is associated with the $\pi-\pi*$ satellite transitions of the aromatic ring in PDA, which suggests that π-π stacking interactions could potentially play a role in the adhesion of PDA onto the GO surface.[40] On the other hand, the N1s spectra of the rGO/PDA-MIP composites are shown in Figure 2I–K. The predominant peak ≈400.0 eV can be decomposed into two Gaussian curve-fitted peaks. The peak at 401.2 eV corresponds to the N—H group from the amine group of PDA's heterocycle; whilst another at 399.6 eV indicates the -N = species, which is derived from the pyridine-like structure of PDA.[41] The above characterization results prove our successful coating of PDA layer onto GO and the partial reduction of GO to rGO.

Figure 3A presents the Thermogravimetric analysis (TGA) for both GO and rGO/PDA-MIP composites over a temperature range of 20 to 800 °C. GO exhibits a complete decomposition at 707 °C, which is attributed to the decomposition of oxygen-containing groups and the pyrolysis of cyclic carbon structures. Conversely, the thermal degradation of rGO/PDA-MIP composites occurs in two phases. First, as temperature escalates, the pyrolysis of oxygen-containing functional groups (e.g., —COOH, —COH, and —C=O) commences at ≈280 °C. Then from 378 °C upward to 800 °C, the rates of decomposition accelerate sharply, predominantly as a consequence of PDA pyrolysis.[42] The final weight losses of rGO/PDA-MIP composites (creatinine/urea/HSA) were 59%, 83%, and 47%, respectively, showing better stability than GO.[43] The different weight losses are mainly attributed to the different degrees of GO reduction and the amount of PDA coating, which can be shown by the Energy Dispersive X-ray Spectroscopy (EDS) mapping results in Figure S3 (Supporting Information). After the PDA coatings, the proportion of O element in the composites decreased, while the content

of N element showed the opposite trend. Among the composites, rGO/PDA-MIP (HSA) presents the most prominent change, which is attributed to the larger amount of PDA coated on the GO surface.

To demonstrate the successful imprinting of templates, the pore size distributions of the rGO/PDA-MIP and rGO/PDA-NIP composites were compared using the Brunauer–Emmett–Teller method (BET) under nitrogen (N_2) adsorption. The adsorption–desorption curves were obtained for the rGO/PDA-MIP composites, as shown in Figure 3B. The hysteresis loops within the relative pressure (P/P_0) range of 0.4–0.9 confirms the existence of the mesoporous nature of the as-prepared material.[44] The shape of the curves is roughly consistent with the H4-type loop, indicating the existence of narrow slit-like pores in the sample based on the lamellar structure of rGO/PDA-MIP composites. The corresponding NIP material on the other hand showed curves of type II, representing non-porous property.[45] As shown in Figure 3C, the pore size distribution studied by the adsorption branch with Barrett–Joyner–Halenda (BJH) method further confirmed the porous nature of the MIPs.[46] The width of mesopores mainly corresponds to the average distance between cavity walls, depending on the size of imprinted cavities in MIPs. In the rGO/PDA-MIP (HSA), a peak appeared with a pore width ≈9.28 nm, which is about the average size of HSA molecules (8–13 nm), indicating the success of HSA imprinting in the MIP layer. However, the peaks ≈2.35 nm shown in three composites were presumed to be false peaks, caused by factors such as the internal tension strength effect of the samples, the connectivity of the pores, the diversity of the pore types, and the dispersion of the pore size, etc.[46] Since the N_2 adsorption isotherm could only provide information for pore sizes between 0.5–200 nm, it is difficult to prove the existence of micropores imprinted by creatinine and urea, which are smaller than 0.5 nm, needing to be characterized through electrochemical methods.[47] Other relevant data including surface area and pore volume are shown in Table S1 (Supporting Information).

The morphology observed using Scanning Electron Microscopy (SEM) and Transmission Electron Microscope (TEM) more intuitively indicated the inference from the above characterization. As shown in Figure 3D, GO shows a typical curved layered structure with a rather smooth surface. After PDA encapsulation (Figure 3E–G), the surface of these composites became rough with a blurred appearance.[48,49] Furthermore, compared with the TEM image of GO (Figure 3H), a small number of mesopores were found on the surface of rGO/PDA-MIP (creatinine) (Figure 3I) and rGO/PDA-MIP (urea) (Figure 3J), which are inferred to be imprinted cavities of partially aggregated small molecules. Whereas for rGO/PDA-MIP (HSA) (Figure 3K), there were a large number of mesopores presented on the surface, which further indicates successful imprinting.

2.3. Electrochemical Behavior of rGO/PDA-MIP Modified Electrodes

Cyclic Voltammetry (CV) was employed to characterize the electrochemical behavior of MIP-modified electrodes.[50] **Figure 4A,B** illustrates the representative CV curves of the rGO/PDA-MIP modified electrodes when utilized for the detection

of small molecules, including creatinine and urea in the $K_3Fe(CN)_6/K_4Fe(CN)_6$ solution. A notable reduction in the peak currents was observed after the electrode surface had been encapsulated with the rGO/PDA-MIP layers. This decline was attributed to the impediment posed by the layer in preventing the $[Fe(CN)_6]^{3-/4-}$ ions from accessing the electrode surface, thus inhibiting the redox current. Following the removal of the template molecules, an increase in the redox current of the CV curves was evident. This suggests that the removal of the templates facilitated the reduction in the resistance of the rGO/PDA-MIP composites, leading to the enhanced redox current. When the targets at 1 ng mL^{-1} were introduced to the solution to interact with the rGO/PDA-MIP, decreases in the redox currents were observed, as the result of the reoccupation of imprinted cavities within the MIP layer, subsequently attenuating the electron transfer of the redox probes, as demonstrated in Figure 4D.

However, we observed a different mechanism for the detection of HSA using rGO/PDA-MIP. As shown in Figure 4C, the redox current decreased after the HSA templates were thoroughly removed, whilst the current increased after the targets recombined with the imprinting cavities. The principle for this phenomenon is reported in Figure 4E. Due to the partial ionization of the amino and carboxyl groups, the HSA molecule carries a large amount of charges. During MIP polymerization, the template molecules were compassed by monomers, with concentrated charged groups surrounded. After the removal of the templates, cavities with negative and positive charges along their surface appeared. Thus, each imprint cavity acts like a spherical capacitor that has been pre-charged, which leads to the obstruction of the redox probe electron transfer. As HSA recognition proceeds, the target and cavity recombines. At this point, a one-to-one response occurs between a pair of charged groups on the protein surface and the cavity wall. The charges on both sides are neutralized, which appears like a "discharging" process of the cavity capacitor.[51] This process reduces the impedance of the composite, which is the main factor affecting the current change in HSA detection, leading to the increased current with the increasing concentration of the HSA target.

As a comparison, the electrochemical behavior of the rGO/PDA-NIP modified electrodes is presented in Figure 4F–H. Upon encapsulating the electrode surface with the rGO/PDA-NIP composites, there was a discernible reduction in the redox current, mirroring the trends observed with the rGO/PDA-MIP modified electrodes. However, subsequent to either the elution process or incubation with the target molecules, the curves essentially exhibited no marked alterations. We attributed this to the lack of imprinted cavities within the rGO/PDA-NIP layer, suggesting that rGO/PDA-NIP is not able to recognize the target. These findings further corroborate the notion that the rGO/PDA-MIP modified electrodes possess the ability to discern target molecules.[33]

2.4. Determination of Biosensing Performance with POC Readout System

RGO/PDA-MIP modified electrodes have been interfaced with the self-designed POC readout system for the detection of creatinine, urea, and HSA at different concentrations. **Figure 5A,B**

**ADVANCED
SCIENCE NEWS**

www.advancedsciencenews.com

**ADVANCED
FUNCTIONAL
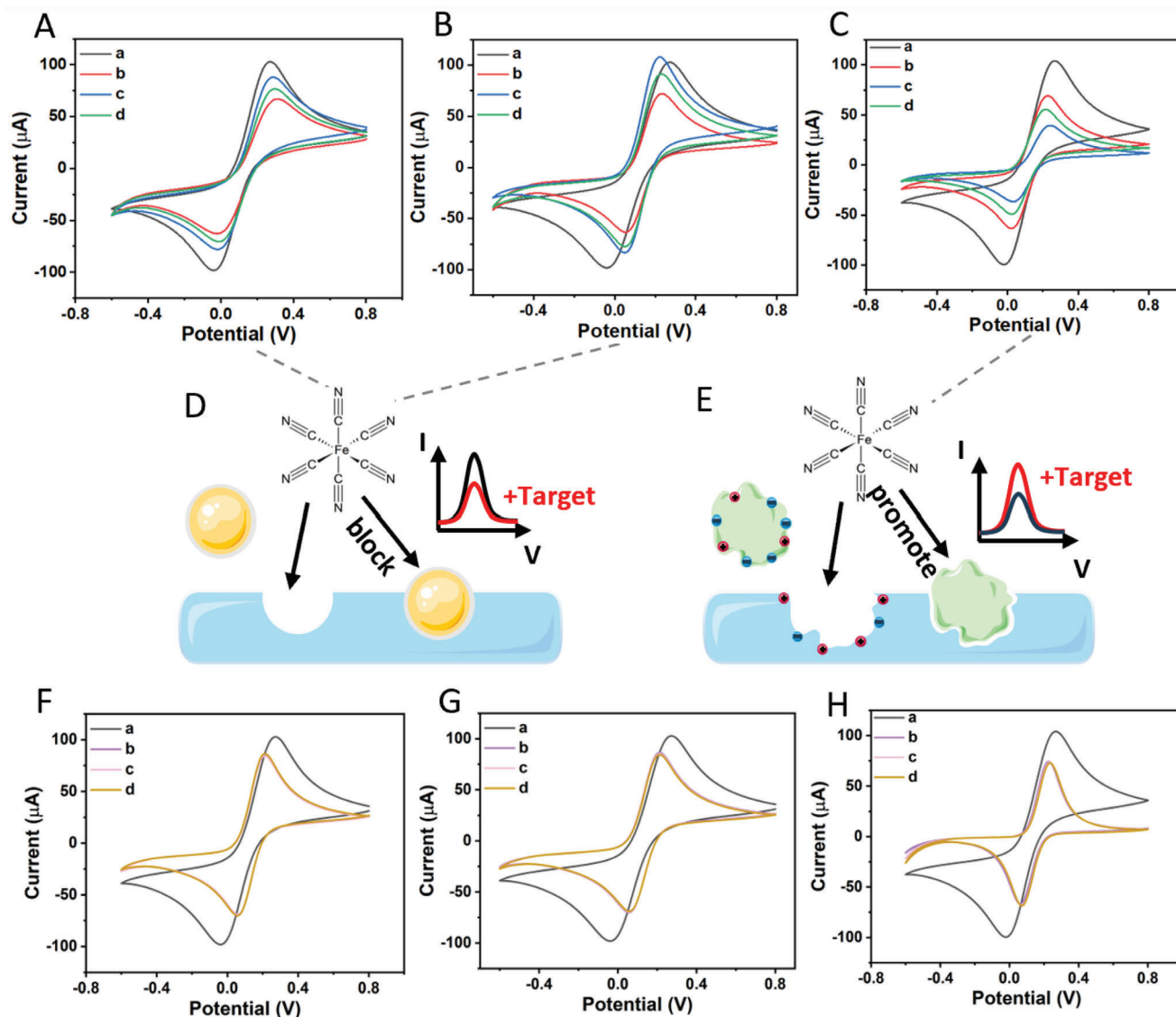MATERIALS**

www.afm-journal.de

Figure 4. Electrochemical behavior of the rGO/PDA-MIP and rGO/PDA-NIP composites modified electrodes. CV curves of A) rGO/PDA-MIP (creatinine), B) rGO/PDA-MIP (urea), C) rGO/PDA-MIP (HSA), F) rGO/PDA-NIP (creatinine), G) rGO/PDA-NIP (urea), H) rGO/PDA-NIP (HSA) modified electrodes, where a: bare electrode, b: composite modified electrode before, and c: after elution, d: incubation with 1 ng mL^{-1} target; Schematic illustration of the detection principle of rGO/PDA-MIP for D) creatinine, urea, and E) HSA detection.

demonstrate that as the creatinine and urea concentrations increase in their detectable ranges respectively, the peak DPV currents decrease, while for HSA detection the curves show the opposite trend as shown in Figure 5C. The calibration plots of Figure 5D–F shows that ΔI increased linearly with the logarithmic concentration of creatinine, urea, and HSA in the range of 10^0–10^{12} 10^2–10^{12} and 10^0–10^8 fg mL^{-1}, with the correlation coefficients of 0.996, 0.998, 0.999, respectively. The accuracy of the calibration plots was ascertained through triplicate determinations, resulting in the relative standard deviation (RSD) value for each concentration being less than 8.2%. The LoD for creatinine, urea, and HSA detection was determined to be 0.27 ± 0.01, 3.87 ± 0.13, and 0.52 ± 0.02 fg mL^{-1} (S/N = 3), respectively.[52] It can be seen that compared to other electrochemical multiplex biosensors (Table S2, Supporting Information), our

biosensor shows extremely low LoDs with wide detection ranges.

Moreover, to evaluate the selectivity of the electrodes modified with rGO/PDA-MIP composites, commonly found potential interferents in human body fluids have been introduced to the electrolyte as a control substances. With respect to the detection of target analytes, Figure 5G,H show that the ΔI measured by rGO/PDA-MIP biosensors for the detection of creatinine and urea was markedly elevated, compared to that for other potential interferents (glucose, glycine, creatine, sarcosine, lactic acid, uric acid, HSA, and ascorbic acid) under an equivalent concentration (1 ng mL^{-1}).[53,54] The maximal recorded ΔI value for the interferent detection was 9.6% of the signal detected for the target analytes. Such findings underscore the outstanding selectivity of rGO/PDA-MIP composites in detecting
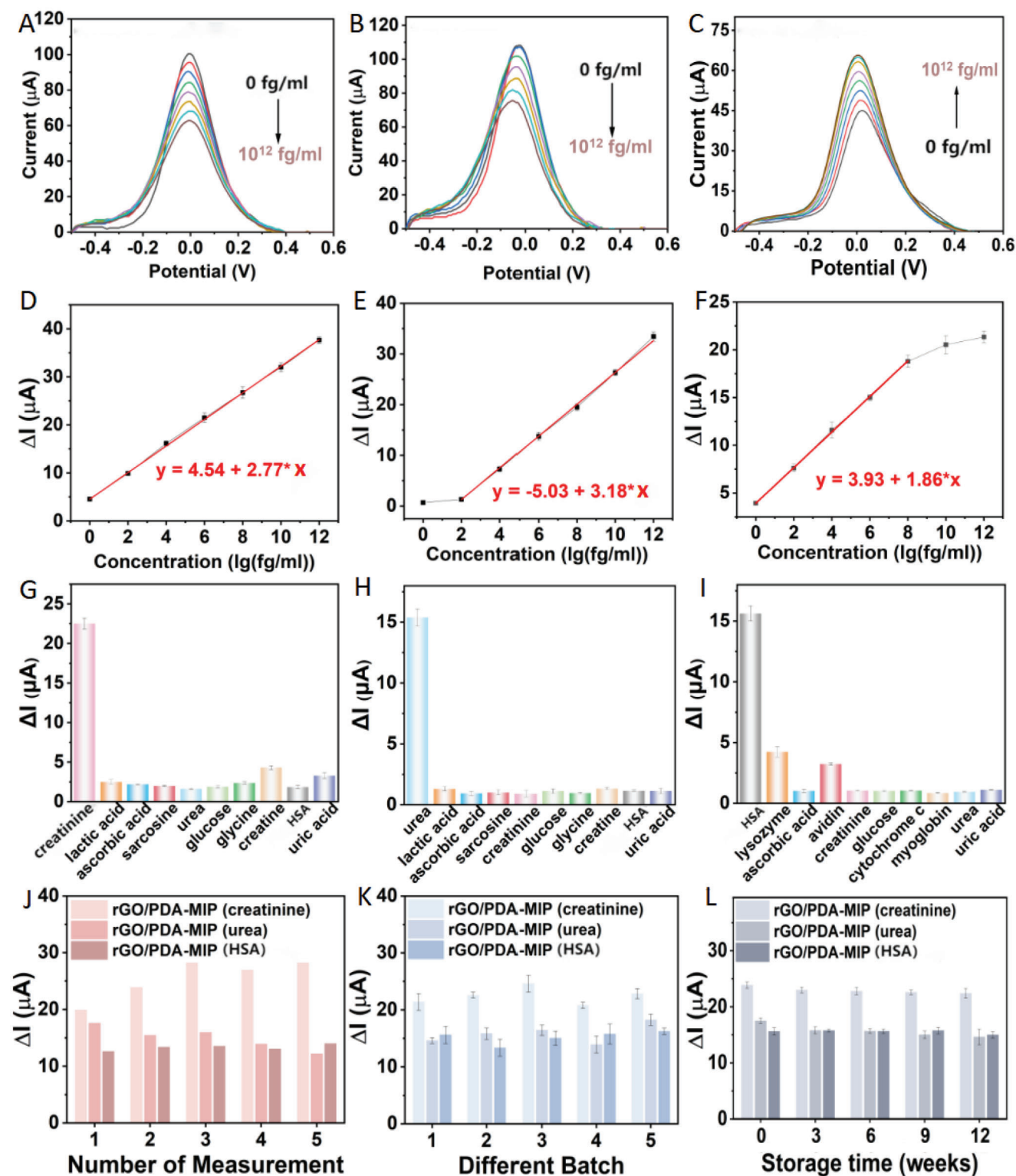
**ADVANCED
SCIENCE NEWS**

www.advancedsciencenews.com

**ADVANCED
FUNCTIONAL
MATERIALS**

www.afm-journal.de

Figure 5. Electrochemical performance of rGO/PDA-MIP modified electrodes for the detection of targets using the POC readout system. The corresponding DPV responses of rGO/PDA-MIP modified electrodes to different concentrations (0, 10^0, 10^2, 10^4, 10^6, 10^8, 10^{10}, and 10^{12} fg mL^{-1}) of A) creatinine, B) urea, and C) HSA in the electrolyte; with their calibration curves of the current values versus the log concentration of D) creatinine, E) urea, F) HSA in the electrolyte. The corresponding values of ΔI of rGO/PDA-MIP modified electrodes to the presence of G) creatinine, H) urea, I) HSA, and other interferents individually at 1 ng mL^{-1}; The value of ΔI to the presence of creatinine, urea, and HSA at 1 ng mL^{-1} individually detected J) in five measurements, K) with five batches of rGO/PDA-MIP composites, L) in three months with rGO/PDA-MIP (creatinine), (urea), (HSA) modified electrodes respectively. Data are presented as mean ± SD (n = 3).

**ADVANCED
SCIENCE NEWS**

www.advancedsciencenews.com

**ADVANCED
FUNCTIONAL
MATERIALS**

www.afm-journal.de

creatinine and urea. As for HSA, Figure 5I demonstrates that common small molecule interferents in body fluids have little effect on its recognition. We also tested the effect of several common interfering proteins including myoglobin, cytochrome c, avidin, and lysozyme on the selectivity of rGO/PDA-MIP (HSA).[55] It can be seen that its selectivity to myoglobin and cytochrome c is excellent, with responses lower than 8.0% of the HSA detection signal. However, its selectivity to lysozyme and avidin was lower, with the response values at 25.2% and 23.6% of that for HSA, respectively. This may be mainly due to the high nonspecific adsorption property of lysozyme and avidin.[56] What's more, myoglobin and cytochrome c mainly being composed of dense α-helices, which makes their structures too rigid to match the HSA imprinted cavities. Differently, the partial sequences of lysozyme consist of flexible random coils, which allows it to partially fit the shape of the HSA recognition cavities and generate nonspecific recognition.[57] Worth noting, during the selectivity test, the concentration of some of the interfering substances was intentionally increased to make them equal with target concentrations. These interferents would only have a negligible impact on the detection of HSA in clinical applications, due to the fact that the concentration of HSA far exceeds that of these potential interfering proteins in human body fluids,[4] which could also be proved by our test results in real human serum and urine samples in the below section (The detailed concentrations of target analytes and common interferents in medically relevant samples were shown in Table S3, Supporting Information.).

Other key biosensing performances were also tested. As depicted in Figure 5J, rGO/PDA-MIP composites were immobilized on the electrodes and reused five times. The continuous increase of ΔI of rGO/PDA-MIP (creatinine) is presumed to be the incomplete removal of creatinine molecules after each wash. The value of ΔI of rGO/PDA-MIP (urea) decreased to 69.3% with the fifth use compared to the first. This could have possibly been due to the partial destruction or detachment of the composite from the electrode surface upon repeated elution. The DPV response of rGO/PDA-MIP (HSA) was 111.9% after five reuses, which demonstrates excellent reusability of the modified electrode. In terms of the reproducibility (batch-to-batch difference), an evaluation across five batches of rGO/PDA-MIP composites was undertaken and shown in Figure 5K, where a commendable reproducibility of rGO/PDA-MIP composites production with a RSD value of less than 7.8% was observed. Moreover, after a three-month storage period at room temperature, the initial response of the electrodes coated with rGO/PDA-MIP retained more than 83.5% of its initial efficacy as reported in Figure 5L. This suggests that to put this sensing platform into commercial application in the future, solutions should be provided for long-term use. From our perspectives, there are two main methods for this condition. First is providing calibration samples for users to calibrate every time before the test. Second is that through testing of large amount of samples with long enough time, we could draw the performance decay curve for the sensor so that users can directly obtain the actual concentration of the analyte based on this curve.

To scrutinize the precision of the POC readout system, the performance of the modified electrodes was concurrently evaluated against the commercial potentiostat (Autolab), as delineated in Figure S4 (Supporting Information). Correspondingly,

Figure S5 (Supporting Information) shows that the peak currents measured by the POC readout system and the Autolab exhibit an excellent linear correlation, with a coefficient (R) greater than 0.994.[58] The detection results show that this POC readout system has reliable performance similar to the large and bulky commercial electrochemical workstation.

2.5. Detection in Clinical Samples with POC Readout System

To verify whether our strategy can be developed for clinical use, we measured analytes concentrations in serum and urine samples from CKD patients and healthy volunteers using our rGO/PDA-MIP multiplex biosensor. To mitigate the influence of fluid viscosity on measurements, the concentrations of the three analytes were determined utilizing spike-and-recovery assays in triplicate, which is the standard practice for clinical settings. All samples for the detection of creatinine and urea were diluted 10^3 times; whilst HSA samples were diluted 10^7 times to match the measuring range of the biosensor. As demonstrated in Table S4 (Supporting Information), the results revealed that the concentration of serum creatinine and urea were much greater in CKD patients compared to healthy volunteers, reaching 2 to 12-fold higher. On the other hand, urinary creatinine and urea were much lower for CKD patients, less than one-half to one-thirteenth of that of healthy volunteers. As for HSA detection, this was not detected in the urine samples from healthy volunteers, whereas was present in all samples from CKD patients, with some patients having urinary albumin concentrations as high as 605 mg L^{-1}.

These results demonstrated significant differences of the chosen targets concentrations between patients with CKD and healthy humans in both serum and urine samples. Moreover, it will be equally meaningful to monitor the changes in concentration of these analytes in body fluids over time to chart the course of CKD in patients. To investigate the accuracy of our proposed method, our detected results were compared with that from a UK nationally accredited university hospital laboratory. As shown in **Figure 6**, the analyte concentrations measured by the hospital were normalized to be 100% for each sample. Compared with the hospital laboratory results, the values obtained with our rGO/PDA-MIP multiplex biosensor had signal percentages between 81.8-119.1% with an RSD value below 7.9% for replicate samples. The signal percentage for the detection of urine albumin levels of healthy volunteers could not be calculated due to its non-existence. However, it can be seen from the post-spiked detection values (Table S4, Supporting Information) that this biosensor could achieve accurate detection of trace albumin in urine, which is of great significance for the early diagnosis and treatment of CKD. The favorable detection results observed in clinical samples indicate that our multiplex biosensor has considerable potential for becoming a valuable POC platform for primary care and health screening programs.

3. Conclusion

In summary, this paper presents an innovative multiplexed POC biosensing system for the ultra-sensitive quantification of

**ADVANCED
SCIENCE NEWS**

www.advancedsciencenews.com

**ADVANCED
FUNCTIONAL
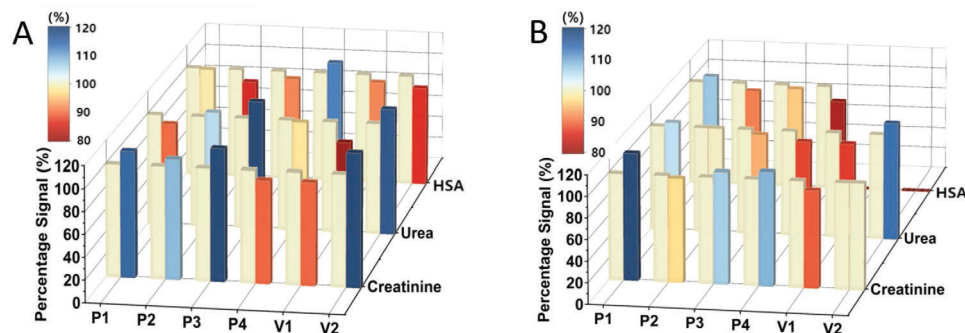MATERIALS**

www.afm-journal.de

Figure 6. Comparison of signal percentage of analytes concentration in A) serum and B) urine from four patients and two volunteers measured by the hospital laboratory and this rGO/PDA-MIP multiplex biosensor. Data are presented as mean ± SD ($n = 3$).

creatinine, urea, and HSA, using the novel rGO/PDA-MIP composites. This rGO/PDA-MIP biosensor demonstrated robust performance, wide linear response range, superior sensitivity and selectivity, unprecedentedly low LoD, and more importantly the capability for the simultaneous detection of multiple CKD biomarkers in human body fluids, which would be important for clinical applications. Our biosensing platform exhibited competitive performance compared to the standard methods used in hospital laboratories, and as such has the potential to be deployed as a POC screening and tracking tool for CKD in primary healthcare settings, health screening programs, and resource-limited regions.

4. Experimental Section

Reagents and Materials: Creatinine was purchased from VWR International. GO water dispersion (0.4 wt%) was purchased from Graphenea (Spain). DA was purchased from Fisher Scientific (UK). Glycine, glucose, urea, uric acid, HSA, creatinine, AP, sarcosine, ethanol, ascorbic acid, sodium dodecyl sulfate (SDS), HCl (37%), H_2SO_4 (95.0-98.0%), lactic acid (85%, FCC), KCl, lysozyme, avidin, cytochrome c, myoglobin, $K_3Fe(CN)_6$, $K_4Fe(CN)_6 \cdot 3H_2O$, phosphate buffer saline (PBS) tablets were purchased from Sigma–Aldrich (UK). All chemicals, unless specified otherwise, were of analytical grade.

Preparation of rGO/PDA-MIP and rGO/PDA-NIP Composites: Creatinine of 35 mg, urea of 30 mg, and HSA of 22.5 mg were added into three vials of 60 mL PBS buffer, which contain DA at 40, 40, and 60 mg, respectively, followed by a stirring at room temperature for 1 h to let the substances form monomer-template complexes. Then 1 mL GO water dispersion at 4 mg mL^{-1} and a suitable amount of oxidant AP ($m_{AP} : m_{DA} = 3:5$) were added to each vial with continuous stirring for 24 h, thus leading the DA-template complex attached to the surface of GO relying on the adhesion property of DA, and at the same time initiating the polymerization process of complex to form surface-MIP composites with embedded templates. The elutions for rGO/PDA-MIP (creatinine/urea/HSA) were then prepared, including 1 M HCl, ethanol and 0.1 M H_2SO_4, and a solution containing 1 M HCl and 0.01 g mL^{-1} SDS, respectively. Finally, the fabricated rGO/PDA-MIP composites with embedded templates were washed with corresponding elution and DI water in succession by repeating the centrifugation and re-suspension to remove the template molecules and the excessive unreacted monomers.

Adsorption Experiments of rGO/PDA-MIP and rGO/PDA-NIP Composites: Each MIPs and NIPs of 1 mg was added to the corresponding set of vials respectively, each of which contained 50 mL of PBS solution and 1 mg of the corresponding target analyte. The dispersions were respectively incubated at room temperature for 10 min under stirring. After reaching the binding equilibrium, the dispersions were centrifuged, with the concentrations of unbinding analytes (creatinine, urea, and HSA) in the supernatant determined at $\lambda = 233, 202, 278$ nm with UV–Vis, respectively.

Characterization of rGO/PDA-MIP and rGO/PDA-NIP Composites: UV–Vis (Shimadzu UV-3600i Plus, Japan) was performed to evaluate and compare the adsorption capacity of fabricated rGO/PDA-MIP and rGO/PDA-NIP composites. Spectra were acquired in the range of 200–800 nm.

Raman spectra (Renishaw inVia, Stockport, UK) were carried out to study the changes in the molecular structure of rGO/PDA-MIP composites at 532 nm laser line, equipped with 10% laser power, 10s exposure time, and an accumulative number of 3 times.

The surface chemical changes were investigated by XPS (Thermo Scientific K-Alpha, USA) employing a monochromatic Al Kα radiation operated at 150 W, with pass energy and step size at 20 and 0.1 eV, respectively. The XPS spectra were referenced to the C1s and N1s line at 284.5 and 399.6 eV, respectively.

FT-IR spectroscopy (PerkinElmer, UK) was obtained to record and compare the characteristic peaks of GO and fabricated rGO/PDA-MIP composites. Samples were scanned in the wavenumber range of 2000–500 cm^{-1}.

The morphology and the surface characteristics of rGO/PDA-MIP composites were investigated by SEM (Hitachi 8230, UK) under 20 kV accelerating voltage and TEM (FEI Talos F2000X) under 200 kV accelerating voltage, respectively. The elemental composition of GO and the as-synthesized rGO/PDA-MIP composites was studied by EDS (Hitachi 8230, Maidenhead, UK) under 20 kV accelerating voltage.

TGA (Perkin–Elmer 4000, Beaconsfield, UK) was operated to detect the weight loss during the pyrolysis of GO and rGO/PDA-MIP composites under N_2 gas flow at a uniform heating rate of 20 °C min^{-1} from 20 to 800 °C.

The comparison of surface area and pore size of the rGO/PDA-MIP and NIP composites was conducted with BET (Micromeritics Instrument Corporation adsorption analyzer, Micromeritics, 3Flex) under 77K, analyzing based on the N_2 adsorption/desorption isotherms.

Design of Electrical Readout System: As shown in **Figure 7A**, the POC readout system was fabricated for multiplex detection of CKD biomarkers. The STM32ch32f103c8t6 (STM32) with ARM architecture was in charge of the control of the whole system, which could be powered by a battery or connection with a laptop through a Micro USB interface. The device was operated through the keys on the panel, including starting detection, setting start and stop potential, and altering step, respectively. After each test, the function of the keys would be changed to displaying curves and peak currents on the screen and uploading the data to a laptop for analyzing, respectively, thereafter restoring when the test is quit.

Figure 7B illustrates the schematic diagram of the electrochemical detector. STM32 was programmed to generate three ramp voltage signals whose sweep range and step could be altered. The voltage signals act on the electrodes and generate response currents, which could then be converted into the detectable voltage signal and processed into current data. The main analog detection circuit of the electrochemical detector is shown in Figure 7C. It consists of four main general-purpose amplifiers, including U1A as the potentiostat, U1B as the current–voltage converter, U1C as

**ADVANCED
SCIENCE NEWS**

www.advancedsciencenews.com

**ADVANCED
FUNCTIONAL
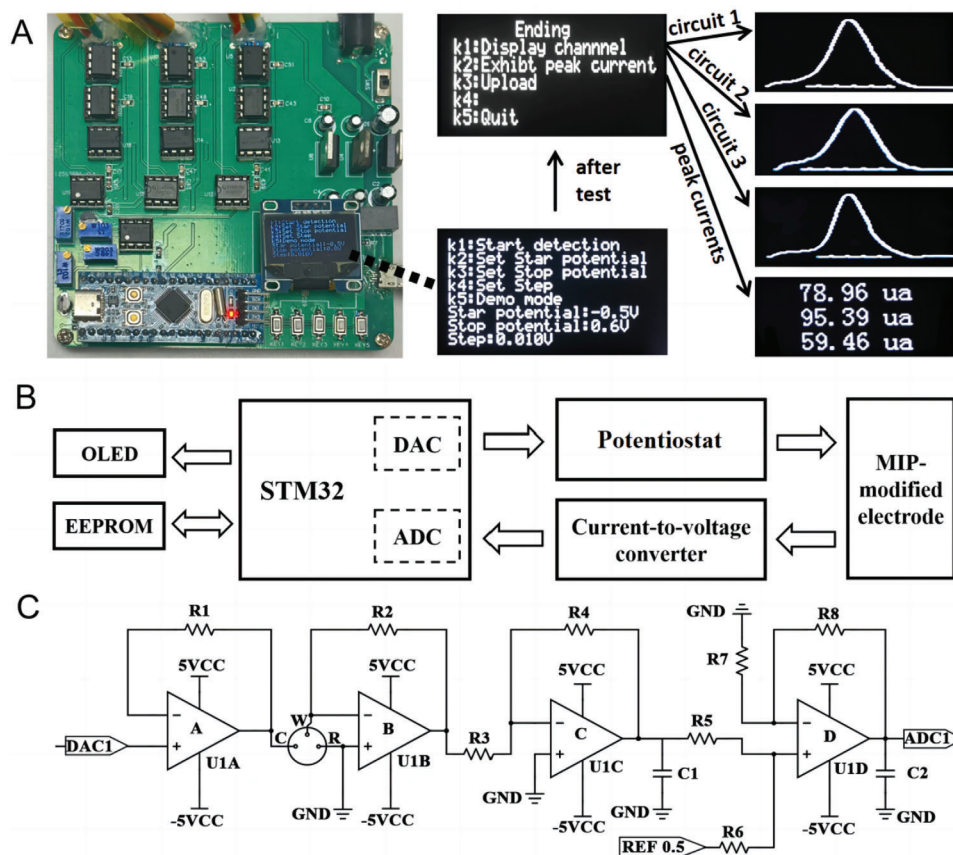MATERIALS**

www.afm-journal.de

Figure 7. Illustration of the POC readout system. A) Optical image of the electrical readout system; B) The block diagram of the electrochemical detector of the POC readout system; C) The main analog detection circuit of the electrochemical detector of the POC readout system.

the voltage inverter, and U1D as the filter and voltage shifter, which are all of model OP07CP. Moreover, R, W, and C in the circuit represent the reference electrode port, working electrode port, and counter electrode port, respectively, connected to the screen-printed carbon electrode (SPCE) by slot. To achieve multiple detection of three biomarkers, other two identical circuits are connected in parallel with it in the POC readout system. The signal in port DAC got from STM32 is stabilized by U1A and applied to port C,[58] generating the DPV voltage signal, which will induce the redox reaction on the working electrode surface. The produced redox current signal can be converted to the voltage signal through U1B and then reversed through U1C. Finally, the voltage signal is biased through U1D fed with 0.5 V reference voltage so that the voltage can be received and digitized at the port ADC of the STM32.

Electrochemical Measurements: SPCEs (DRP-110, Metrohm) were used as the substrate electrodes. The SPCE modified with 20 µL of prepared rGO/PDA-MIP dispersion (10 mg mL^{-1}) will be generated using the drop-cast self-assembly process, then immersed in the electrolyte containing 0.01 M PBS solution (pH = 7.4), 5 mM Fe(CN)$_6^{3-/4-}$, 0.1 M KCl, and corresponding analyte. Electrochemical measurements will be performed after 10 min incubation time of the modified electrodes. The electrochemical behavior and performance of the rGO/PDA-MIP modified electrodes were characterized by CV and DPV, respectively. CV was implemented under a scan rate of 50 mV s^{-1} over the potential range between -0.6 and $+0.8$ V with an electrochemical workstation (Autolab (PGSTAT204, Metrohm)). DPV was implemented under a scan rate of 20 mV s^{-1} with the step of 10 mV over the potential range between -0.5 and $+0.6$ V with both the self-designed readout system and Autolab as a control experiment. All potentials mentioned were referred to the Ag reference electrode in SPCE.

Human Samples: Ethical approval for research was secured from the research ethics committee to obtain serum and urine samples from unidentified patients, who were diagnosed with renal disease, alongside healthy volunteers (UK National Research Ethics 23/NW/0230). Patients' body fluids were provided from Royal Free Hospital in London, including four of each blood and urine samples, all in 5 mL. The inclusion criteria of patients were age between 18 and 80 at the time of diagnosis of moderate to severe CKD. After 30 min at room temperature, blood samples were centrifuged at 3000 rpm for 3 min to get the serum, frozen at -80 °C together with urine samples. The healthy control serum and urine samples with two of each also in 5 mL were provided by healthy volunteers, same pre-preparing procedure and storage environment as that of patients' samples. Samples for the detection of creatinine and urea were diluted 10^3 times, while samples for the HSA test were diluted 10^7 times, thus leading to the diluted concentration within the measuring range of the corresponding rGO/PDA-MIP composites.

Statistical Analysis: The analyte concentrations in human serum and urine measured by the hospital were normalized to be 100% for each sample for the calculation of the detection recovery rate. Error bars represent the standard deviation of the mean, with all data presented as mean ± SD. All the sample size (n) for each analysis was contained in the figure legends. All the experiments were done in triplicate. All data were analyzed with OriginPro 2023b software.

Supporting Information

Supporting Information is available from the Wiley Online Library or from the author.

**ADVANCED
SCIENCE NEWS**

www.advancedsciencenews.com

**ADVANCED
FUNCTIONAL
MATERIALS**

www.afm-journal.de

Acknowledgements

Conflict of Interest

The authors declare no conflict of interest.

Author Contributions

Y.-X.L. was involved with conceptualization, visualization, investigation, formal analysis, data curation, and wrote the original draft. L.L. was involved with performing experiments and data curation. S.G. was involved with providing resources. Y.K., Y.-J.L., and X.G. were involved with the methodology. X.L. was involved with data curation. E.Y. was involved with methodology and wrote, reviewed, and edited the final manuscript. A.D. was involved with providing resources and wrote, reviewed, and edited the final manuscript. Y.L. was involved with supervision and wrote, reviewed, and edited the final manuscript. B.L. was involved with conceptualization, supervision, providing resources, and funding acquisition and wrote the original draft, and wrote, reviewed, and edited the final manuscript.

Data Availability Statement

The data that support the findings of this study are available from the corresponding author upon reasonable request.

Keywords

[1] K. Amreen, K. Guha, S. Goel, *Next Generation Smart Nano-Bio-Devices*, Springer, Berlin **2022**, pp. 81–101.

[2] N. R. Hill, S. T. Fatoba, J. L. Oke, J. A. Hirst, C. A. O'Callaghan, D. S. Lasserson, F. R. Hobbs, *PloS one* **2016**, *11*, e0158765.

[3] S. Sena, D. Syed, R. Romeo, G. Krzymowski, R. McComb, *Clin. Chem.* **1988**, *34*, 2144.

[4] T.-Y. Lin, C.-H. Hu, T.-C. Chou, *Biosens. Bioelectron.* **2004**, *20*, 75.

[5] W. D. Comper, T. M. Osicka, *Adv. Chronic Kidney Dis.* **2005**, *12*, 170.

[6] M. M. Melo, A. Machado, A. O. Rangel, R. B. Mesquita, *Chemosensors* **2023**, *11*, 368.

[7] N. J. Langenfeld, L. E. Payne, B. Bugbee, *PLoS One* **2021**, *16*, e0259760.

[8] J. P. E. Cassol, R. Scolari, R. N. Moresco, *Anal. Biochem.* **2021**, *614*, 114047.

[9] C. F. Poole, S. K. Poole, *Chromatography today*, Elsevier, Amsterdam, Netherlands **2012**.

[10] I. Lewińska, M. Speichert, M. Granica, Ł. Tymecki, *Sens. Actuators, B* **2021**, *340*, 129915.

[11] Y. Liu, X. Luo, Y. Dong, M. Hui, L. Xu, H. Li, J. Lv, L. Yang, Y. Cui, *Anal. Chim. Acta* **2022**, *1227*, 340264.

[12] B. Öndeş, F. Akpınar, M. Uygun, M. Muti, D. A. Uygun, *Microchem. J.* **2021**, *160*, 105667.

[13] J. Yoon, Y. S. Yoon, D.-J. Kim, *ACS Appl. Nano Mater.* **2020**, *3*, 7651.

[14] W. Xiao, Y. Li, Y. Xiong, Z. Chen, H. Li, *Anal. Bioanal. Chem.* **2023**, *415*, 3363.

[15] F. T. Cavalcante, I. R. de A. Falcão, J. E. da S. Souza, T. G. Rocha, I. G. de Sousa, A. L. Cavalcante, A. L. de Oliveira, M. C. de Sousa, J. C. dos Santos, *Electrochem* **2021**, *2*, 149.

[16] M. Pan, J. Yang, K. Liu, Z. Yin, T. Ma, S. Liu, L. Xu, S. Wang, *Nanomaterials* **2020**, *10*, 209.

[17] M. van Schrojenstein Lantman, A.-E. van de Logt, E. Prudon-Rosmulder, M. Langelaan, A. Y. Demir, S. Kurstjens, A. van der Horst, A. Kuypers, A. Greuter, J. Kootstra-Ros, *Clin. Chem. Lab. Med. (CCLM)* **2023**, *61*, 2167.

[18] B. G. Rosa, O. E. Akingbade, X. Guo, L. Gonzalez-Macia, M. A. Crone, L. P. Cameron, P. Freemont, K.-L. Choy, F. Güder, E. Yeatman, *Biosens. Bioelectron.* **2022**, *203*, 114050.

[19] N. Bagheri, A. Khataee, B. Habibi, J. Hassanzadeh, *Talanta* **2018**, *179*, 710.

[20] M. M. El-Beshlawy, F. M. Abdel-Haleem, A. Barhoum, *Electroanalysis* **2021**, *33*, 1244.

[21] J. J. BelBruno, *Chem. Rev.* **2018**, *119*, 94.

[22] Y. Li, L. Luo, Y. Kong, Y. Li, Q. Wang, M. Wang, Y. Li, A. Davenport, B. Li, *Biosens. Bioelectron.* **2024**, *249*, 116018.

[23] T. Alizadeh, Z. Mousavi, *Microchim. Acta* **2022**, *189*, 393.

[24] E. Rajaee, M. Izadyar, M. R. Housaindokht, *Mol. Syst. Des. Eng.* **2023**, *8*, 1182.

[25] J. Ma, Y. Zhang, H. Sun, P. Ding, D. Chen, *J. Mater. Chem. B* **2022**, *10*, 4226.

[26] C. Dong, H. Shi, Y. Han, Y. Yang, R. Wang, J. Men, *Eur. Polym. J.* **2021**, *145*, 110231.

[27] B. Li, G. Pan, N. D. Avent, K. Islam, S. Awan, P. Davey, *J. Nanosci. Nanotechnol.* **2016**, *16*, 12805.

[28] Y. Hou, C.-C. Lv, Y.-L. Guo, X.-H. Ma, W. Liu, Y. Jin, B.-X. Li, M. Yang, S.-Y. Yao, *Journal of Analysis and Testing* **2022**, *6*, 247.

[29] Z.-Z. Yin, S.-W. Cheng, L.-B. Xu, H.-Y. Liu, K. Huang, L. Li, Y.-Y. Zhai, Y.-B. Zeng, H.-Q. Liu, Y. Shao, *Biosens. Bioelectron.* **2018**, *100*, 565.

[30] P. Li, Z. Liu, Z. Yan, X. Wang, E. M. Akinoglu, M. Jin, G. Zhou, L. Shui, *J. Electrochem. Soc.* **2019**, *166*, B821.

[31] Z. M. Karazan, M. Roushani, *Talanta* **2022**, *246*, 123491.

[32] Y. Sun, H. Du, Y. Lan, W. Wang, Y. Liang, C. Feng, M. Yang, *Biosens. Bioelectron.* **2016**, *77*, 894.

[33] W. Liu, Y. Ma, G. Sun, S. Wang, J. Deng, H. Wei, *Biosens. Bioelectron.* **2017**, *92*, 305.

[34] X. Liu, H. Andersen, Y. Lu, B. Wen, I. P. Parkin, M. De Volder, B. D. Boruah, *ACS Appl. Mater. Interfaces* **2023**, *15*, 6963.

[35] B. Li, G. Zhang, I. B. Tahirbegi, M. J. Morten, H. Tan, *Electrochem. Commun.* **2021**, *123*, 106927.

[36] A. Y. Lee, K. Yang, N. D. Anh, C. Park, S. M. Lee, T. G. Lee, M. S. Jeong, *Appl. Surf. Sci.* **2021**, *536*, 147990.

[37] I. Kaminska, W. Qi, A. Barras, J. Sobczak, J. Niedziolka-Jonsson, P. Woisel, J. Lyskawa, W. Laure, M. Opallo, M. Li, *Chemistry* **2013**, *19*, 8673.

[38] Y.-M. Ha, Y. N. Kim, Y. C. Jung, *Polymers* **2021**, *13*, 1274.

[39] L. Luo, H. Huang, Y. Yang, S. Gong, Y. Li, Y. Wang, W. Luo, Z. Li, *Appl. Surf. Sci.* **2022**, *575*, 151699.

[40] W. Ye, Y. Chen, Y. Zhou, J. Fu, W. Wu, D. Gao, F. Zhou, C. Wang, D. Xue, *Electrochim. Acta* **2014**, *142*, 18.

[41] Y. Liu, W. Tu, M. Chen, L. Ma, B. Yang, Q. Liang, Y. Chen, *Chem. Eng. J.* **2018**, *336*, 263.

[42] A. Alkhouzaam, H. Qiblawey, M. Khraisheh, *Membranes* **2021**, *11*, 86.

[43] F. Chang, H. Wang, S. He, Y. Gu, W. Zhu, T. Li, R. Ma, R. S. C. Adv, **2021**, *11*, 31950.

**ADVANCED
SCIENCE NEWS**

www.advancedsciencenews.com

**ADVANCED
FUNCTIONAL
MATERIALS**

www.afm-journal.de

[44] A. Crake, K. C. Christoforidis, A. Gregg, B. Moss, A. Kafizas, C. Petit, *Small* **2019**, *15*, 1805473.

[45] C. Sangwichien, G. Aranovich, M. Donohue, *Colloids Surf. A* **2002**, *206*, 313.

[46] R. J. Krupadam, M. S. Khan, S. R. Wate, *Water Res.* **2010**, *44*, 681.

[47] R. Bardestani, G. S. Patience, S. Kaliaguine, *Can J Chem Eng* **2019**, *97*, 2781.

[48] J. Luo, S. Jiang, X. Liu, *J. Phys. Chem. C* **2013**, *117*, 18448.

[49] L. Luo, Y. Liu, S. Chen, Q. Zhu, D. Zhang, Y. Fu, J. Li, J. Han, S. Gong, *Small* **2023**, 2308756.

[50] Y. Li, L. Luo, M. Nie, A. Davenport, Y. Li, B. Li, K.-L. Choy, *Biosens. Bioelectron.* **2022**, *216*, 114638.

[51] K. Ghanbari, M. Roushani, *Sens. Actuators, B* **2018**, *258*, 1066.

[52] S. Liu, Y. Ma, M. Cui, X. Luo, *Sens. Actuators, B* **2018**, *255*, 2568.

[53] K. K. Reddy, K. V. Gobi, *Sens. Actuators, B* **2013**, *183*, 356.

[54] T. Wen, W. Zhu, C. Xue, J. Wu, Q. Han, X. Wang, X. Zhou, H. Jiang, *Biosens. Bioelectron.* **2014**, *56*, 180.

[55] Z. Stojanovic, J. Erdőssy, K. Keltai, F. W. Scheller, R. E. Gyurcsányi, *Anal. Chim. Acta* **2017**, *977*, 1.

[56] M. Ide, A. Mitamura, T. Miyashita, *Bull. Chem. Soc. Jpn.* **2001**, *74*, 1355.

[57] M. Cieplak, K. Szwabinska, M. Sosnowska, B. K. Chandra, P. Borowicz, K. Noworyta, F. D'Souza, W. Kutner, *Biosens. Bioelectron.* **2015**, *74*, 960.

[58] Y. Fan, J. Liu, Y. Wang, J. Luo, H. Xu, S. Xu, X. Cai, *Biosens. Bioelectron.* **2017**, *95*, 60.